# C(sp³)–H Fluorination with a Copper(II)/(III) Redox Couple

Jamey K. Bower,[†] Andrew D. Cypcar,[†] Brenda Henriquez,[‡] S. Chantal. E. Stieber,*[‡] and Shiyu Zhang*[†]

[†]Department of Chemistry & Biochemistry, The Ohio State University, 100 West 18th Avenue, Columbus, Ohio 43210, United States

[‡]Department of Chemistry & Biochemistry, California State Polytechnic University, Pomona, 3801 West Temple Avenue, Pomona, California 91768, United States

**ABSTRACT:** Despite the growing interest in the synthesis of fluorinated organic compounds, few reactions are able to incorporate fluoride ion directly into alkyl C−H bonds. Here, we report the C(sp³)−H fluorination reactivity of a formally copper(III) fluoride complex. The C−H fluorination intermediate, **L**CuF, along with its chloride and bromide analogs, **L**CuCl and **L**CuBr, were prepared directly from halide sources with a chemical oxidant and fully characterized with single-crystal X-ray diffraction, X-ray absorption spectroscopy, UV-Vis spectroscopy, and $^1$H nuclear magnetic resonance spectroscopy. Quantum chemical calculations reveal significant halide radical character for all complexes, suggesting their ability to initiate and terminate a C(sp³)-H halogenation sequence by sequential hydrogen atom abstraction (HAA) and radical capture. The capability of HAA by the formally copper(III) halide complexes was explored with 9,10-dihydroanthracene, revealing that **L**CuF exhibits rates two orders of magnitude higher than **L**CuCl and **L**CuBr. In contrast, all three complexes efficiently capture carbon radicals to afford C(sp³)−halogen bonds. Mechanistic investigation of radical capture with trityl radical revealed that **L**CuF proceeds through a concerted mechanism, while **L**CuCl and **L**CuBr follow a stepwise electron transfer-halide transfer pathway. The capability of **L**CuF to perform both hydrogen atom abstraction and radical capture was leveraged to enable fluorination of allylic and benzylic C−H bonds and α-C−H bonds of ethers at room temperature.

## INTRODUCTION

Carbon-fluorine bonds are becoming increasingly prevalent in pharmaceuticals and agrochemicals.[1] The value of fluorinated compounds in these applications stems from their enhancement of lipophilicity, metabolic stability, and receptor binding affinity.[2] Given the abundance of C(sp³)–H bonds in organic molecules, the atom-efficient conversion of C(sp³)-H to C(sp³)-F bonds has been a prominent goal for synthetic methodology development.[3–6] The majority of C(sp³)-H fluorination methods employ a radical approach that depends on electrophilic fluorination reagents, e.g. Selectfluor,[7–12] and N-fluorosulfonimide (NFSI),[13–15] to react directly with alkyl radicals to afford C(sp³)–F bonds (Figure 1a).[16,17] Few C(sp³)–H fluorination protocols employ metal-based, nucleophilic fluorine ($F^-$) sources, i.e. metal fluorides,[3] to deliver the C(sp³)-F bond, as most notably demonstrated by Groves and colleagues.[18,19] Practically, the metal-fluoride-mediated process is advantageous, since it is more suitable for $^{18}$F radiolabeling and controlling the stereochemistry of the C(sp³)–F center.[20–22] Despite this progress, a remaining challenge is improving the selectivity of alkyl fluorination.[1] As chiral copper complexes are well-known asymmetric catalysts for radical C–H functionalization,[23–25] the use of tunable copper fluoride complexes, in principle, would provide the opportunity to further improve the selectivity of C(sp³)–H fluorination. However, the mechanistic step of R• capture at a copper fluoride complex to afford C(sp³)–F bonds has yet to be established.

While copper(II) chloride and bromide are well-documented C(sp³)–H halogenating reagents,[26–28] copper(II) fluoride is not amenable to analogous fluorination reactivity, likely due to the highly ionic nature of the $Cu^{II}$-F bond (Figure 1b). Further underscoring this concept, Lectka and co-workers reported the C(sp³)-H fluorination of unactivated alkanes employing a copper(I) source and Selectfluor.[7] Mechanistic studies revealed that the copper(I) complex serves to initiate the reaction through the formation of an inert copper(II) fluoride while Selectfluor mediates the key C(sp³)-F bond forming step.[29] Thus, we questioned whether a more covalent Cu-F bond might enable C(sp³)–H fluorination at the copper center. Specifically, we envisioned the case of a formally $[Cu^{III}\text{-}F]^{2+}$ complex. Oxidation of a copper(II) fluoride to copper(III) would increase the copper effective nuclear charge and lower the Cu d orbital energy to allow for increased fluorine contribution to the lowest unoccupied molecular orbital (LUMO) of the $[Cu^{III}\text{-}F]^{2+}$ motif (Figure 1b). Consistent with this hypothesis, recent X-ray absorption spectroscopy studies on formally copper(III) complexes showed that a majority of LUMOs are located on the ligand instead of the metal, resulting in an inverted ligand field.[30,31] The increased hole character on the ligand has been invoked to explain the C(sp³)–H amination reactivity of Cu nitrene complexes.[32,33] Thus, we propose that the introduction of fluorine hole character will allow a $[Cu^{III}\text{-}F]^{2+}$ complex to perform both hydrogen atom abstraction (HAA) and radical capture (RC) to furnish the C(sp³)–F bond (Figure 1c). Herein, we report the synthesis of formally copper(III) fluoride, chloride, and bromide complexes and detailed mechanistic investigation of their C(sp³)-H halogenation reactivity. While all $[Cu^{III}\text{-}X]^{2+}$ complexes are proficient at radical capture, the $[Cu^{III}\text{-}F]^{2+}$ complex is faster at HAA than $[Cu^{III}\text{-}Cl]^{2+}$ and

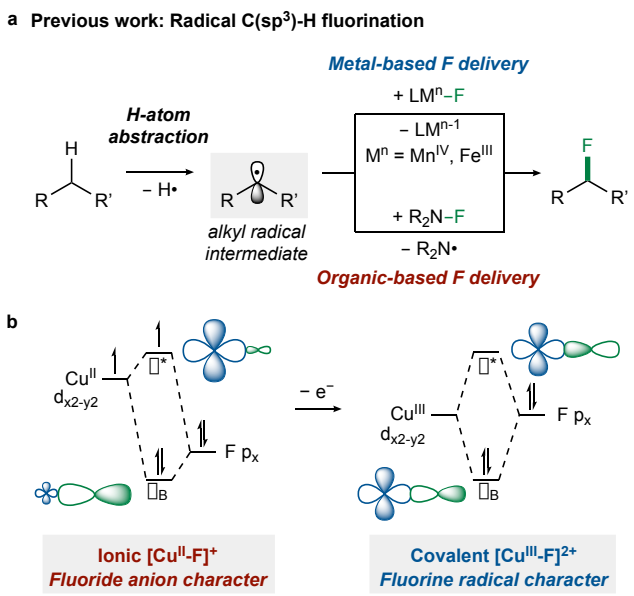


**Figure 1.** (a) Radical C($sp^3$)–H fluorination by metal- and organic-mediated approaches. (b) Oxidation of a copper(II) fluoride to formally copper(III) increases the covalency of the Cu-F bond and the hole character on F. (c) Direct C($sp^3$)–H fluorination by sequential hydrogen atom abstraction and radical capture with a formally copper(III) fluoride complex.

$[Cu^{III}\text{-Br}]^{2+}$ complexes by two orders of magnitude. Leveraging these mechanistic insights, we demonstrate that the copper(III) fluoride is capable of directly fluorinating allylic and benzylic C($sp^3$)–H bonds as well as α-C–H bonds of ethers at room temperature using $F^-$ as the fluorine source.

## RESULTS AND DISCUSSION

**Synthesis, Characterization, and Electronic Structure of Formally Copper(III) Halides.** To examine the ability of the $[Cu^{III}\text{-F}]^{2+}$ motif to fluorinate C($sp^3$)–H bonds, we set out to synthesize a discrete $[Cu^{III}\text{-F}]^{2+}$ complex. Additionally, we targeted copper(III) chloride and bromide analogs to provide a detailed understanding of how electronic structure affects reactivity relevant to C($sp^3$)–H halogenation across the copper(III) halide series. To support the one-electron $Cu^{II}/Cu^{III}$ redox couple central to our hypothesis, we selected the biscarboxamidopyridine ligand (**L** = [N-N'-bis(2,6-diisopropylphenyl)-2,6-pyridinedicarboxamido]$^{2-}$) based on the work by Tolman and co-workers.[34] Reaction of **L**$Cu^{II}$(MeCN) with tetrabutylammonium halide ([TBA]X) salts in tetrahydrofuran afforded the corresponding anionic copper(II) halide complexes [TBA]**L**$Cu^{II}$X (X = F, Cl, Br) in 88%, 83%, and 84% yield, respectively (Scheme 1). All [TBA]**L**$Cu^{II}$X complexes were characterized by X-ray crystallography and electron paramagnetic resonance (see Supplementary Information), confirming copper $S = ½$ centers. Samples of [TBA]**L**$Cu^{II}$F were unsuitable for single crystal X-ray diffraction, therefore, the bis(triphenylphosphine)iminium (PPN) salt, [PPN]**L**$Cu^{II}$F, was prepared to obtain structural characterization (Figure S1). The copper(II) halide structures

**Scheme 1. Synthesis of anionic copper(II) halides**

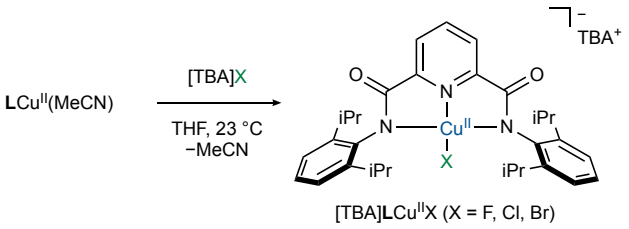


exhibit similar Cu-N distances between **L** and the copper center (Cu-$N_{(avg)}$ (Å) = 1.977 for $[\mathbf{L}Cu^{II}F]^-$, 1.987 for $[\mathbf{L}Cu^{II}Cl]^-$, 1.982 for $[\mathbf{L}Cu^{II}Br]^-$). All copper(II) centers adopt a distorted square planar geometry ($\tau_4$ = 0.15 for $[\mathbf{L}Cu^{II}F]^-$), 0.20 for $[\mathbf{L}Cu^{II}Cl]^-$), 0.20 for $[\mathbf{L}Cu^{II}Br]^-$, $\tau_4$ = 0 for square planar, $\tau_4$ = 1 for tetrahedral)[35] with the halide positioned slightly out of the $N_3Cu$ plane. Seeking to access copper(III) halides by one-electron oxidation, we measured the $Cu^{II}/Cu^{III}$ redox potential in solution. The cyclic voltammograms of [TBA]**L**$Cu^{II}$X complexes in $CH_2Cl_2$ exhibit quasi-reversible redox couples at $E_{1/2}$ = 0.465 V for $[\mathbf{L}Cu^{II}F]^-$, 0.525 V for $[\mathbf{L}Cu^{II}Cl]^-$, and 0.525 V for $[\mathbf{L}Cu^{II}Br]^-$ (vs $Ag/AgNO_3$, Figures S2-S4), respectively. As expected, [TBA]**L**$Cu^{II}$F features the most cathodic redox potential due to the high electronegativity of fluoride. Interestingly, [TBA]**L**$Cu^{II}$Br is oxidized at nearly the same potential as [TBA]**L**$Cu^{II}$Cl but features the most reversible redox profile of the series, with a peak-to-peak separation of 160 mV.

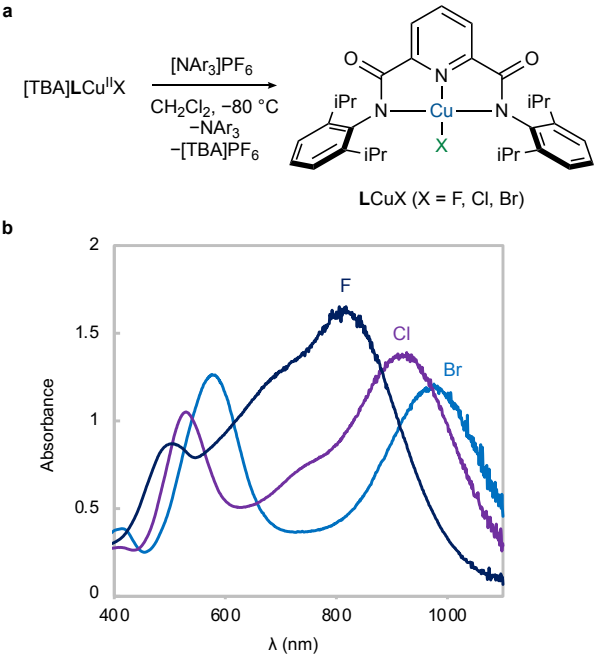


**Figure 2.** (a) Synthesis of formally copper(III) halides by chemical oxidation of the copper(II) halide precursor with $[NAr_3]PF_6$ (Ar = 4-bromophenyl). (b) Overlay of the UV-Vis spectra of **L**CuF, **L**CuCl, and **L**CuBr at −80 °C in $CH_2Cl_2$ (0.1mM).

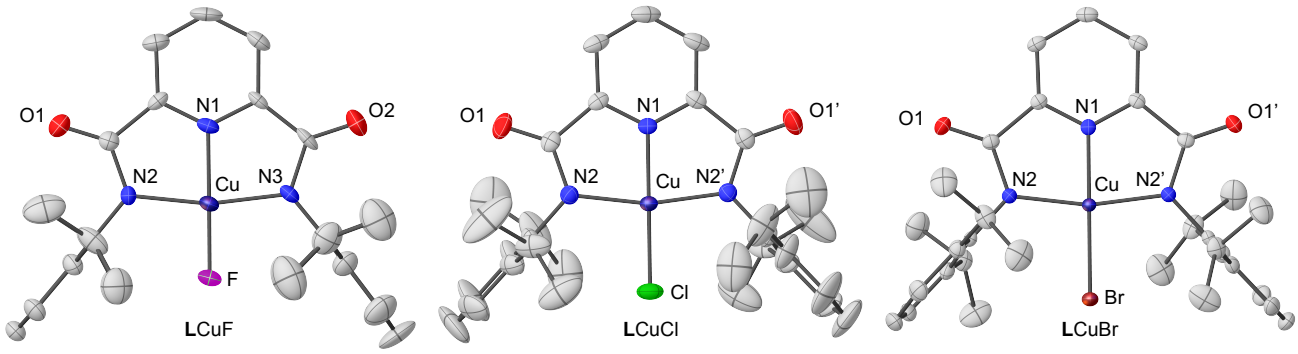


**Figure 3.** Solid-state structures of **L**CuF, **L**CuCl, and **L**CuBr with thermal ellipsoids shown at 50% level of probability. Cocrystallized solvents and minor components of disorder are omitted for clarity. Selected bond lengths (Å) and angles (°): **L**CuF Cu-F = 1.755(3); Cu-$N_1$ = 1.841(4); Cu-$N_2$ = 1.901(4); $N_1$-Cu-F = 179.68(17). **L**CuCl Cu-Cl = 2.1085(8); Cu-$N_1$ = 1.859(2); Cu-$N_2$/$N_2$' = 1.9132(16); $N_1$-Cu-Cl = 180. **L**CuBr Cu-Br = 2.2562(4); Cu-$N_1$ = 1.8623(18); Cu-$N_2$/$N_2$' = 1.9159(13); $N_1$-Cu-Br = 180.

Variable temperature UV-Vis spectrophotometry was utilized to study the thermal stability of the copper(III) fluoride complex, **L**CuF. Based on the CV profiles of [TBA]**L**$Cu^{II}$X, the aminium radical cation, [$NAr_3$]$PF_6$ (Ar = 4-bromophenyl; $E_{1/2}$ = 0.66 V vs Ag/$AgNO_3$ in MeCN) was selected as the chemical oxidant to prepare **L**CuX complexes (Figure 2a). Treatment of [TBA]**L**$Cu^{II}$F with [$NAr_3$]$PF_6$ at −80 °C in $CH_2Cl_2$ resulted in the rapid formation of a new species with intense absorptions at 520 nm (ε = 9100 $M^{-1}$ $cm^{-1}$) and 820 nm (ε = 18600 $M^{-1}$ $cm^{-1}$), which were attributed to the **L**CuF complex (Figure 2b). The UV-Vis spectra of **L**CuCl and **L**CuBr, prepared analogously via chemical oxidation, share the two main charge transfer bands (Figure 2b). Both UV-Vis bands red-shift along the series from **L**CuF to **L**CuCl to **L**CuBr in accordance with the donating ability of the halide ligands, indicating that these transitions correspond to ligand-to-metal charge transfer (LMCT).[36] Time-dependent density functional theory (TD-DFT) calculations at B3LYP/def2-TZVP(-f) level reproduced the two intense features as well as their red-shifting trends (Figure S48). Both absorptions originate from charge transfers from halide/**L** based orbitals to the LUMO, which features the σ* interaction of the Cu $d_{x2-y2}$ and the halide/**L**. The TD-DFT calculations also suggest that decreasing peak intensity from **L**CuF to **L**CuCl to **L**CuBr correlates to the reducing contribution of **L** to the donor orbital (Table S7-S9). While **L**CuCl and **L**CuBr are stable in $CH_2Cl_2$ at 20 °C, **L**CuF undergoes slow decay at temperatures above −20 °C. The $^1$H nuclear magnetic resonance (NMR) spectra of **L**CuX in $CD_2Cl_2$ show sharp resonances within the 0-9 ppm range that account for all ligand protons (Figures S18-S23), consistent with a diamagnetic ground state for **L**CuX complexes. Additionally, a $^{19}$F NMR signal at −209.4 ppm is observed for **L**CuF.

Single crystal X-ray diffraction confirmed the formation of [$Cu^{III}$-X]$^{2+}$ species (Figure 3). The Cu-N and Cu-X bond distances contract by 0.07-0.1 Å upon oxidation from $Cu^{II}$ to the formally $Cu^{III}$ state. All copper(III) complexes exhibit more rigid square planar geometries ($\tau_4$ = 0.09 for **L**CuF, 0.10 for **L**CuCl, 0.10 for **L**CuBr) compared to their copper(II) counterparts. Overall, the structural reorganization upon oxidation is minimal, consistent with the highly reversible redox couples observed by CV (Figures S2-S4). **L**CuF is, to the best of our knowledge, the first structurally characterized, discrete copper(III) fluoride complex and features the shortest Cu-F distance (1.755(3) Å) reported in the Cambridge Structural Database. Furthermore, **L**CuCl and **L**CuBr feature shorter Cu-Cl (2.1085(8) Å) and Cu-Br (2.2562(4) Å) bonds than previously reported five-coordinate copper(III) halide complexes (Cl: 2.2011(18) – 2.468(1) Å; Br: 2.3842(5) – 2.600(1) Å).[31,36–38]

X-ray absorption spectroscopy (XAS) of the copper K-edge shows a rising edge shift of 1.4 eV upon oxidation of the $Cu^{II}$-F, $Cu^{II}$-Cl, and $Cu^{II}$-Br precursors, consistent with a more oxidized copper center (Figure 4, Figures S37-S38). The edge shift of 1-3 eV is in the range of reported values for oxidation from $Cu^{II}$ to $Cu^{III}$.[39,40] Similarly, the pre-edge features are shifted from ca. 8979 eV for the $Cu^{II}$ species to ca. 8981 eV for the $Cu^{III}$ complexes. The edges of both F complexes are also shifted to higher energy than the analogous Cl complexes, consistent with the shorter Cu-F bonds observed crystallographically. Lancaster and coworkers have argued that most formally copper(III) complexes have a LUMO that resides predominantly on the ligands instead of the Cu $d_{x2-y2}$ orbital, suggesting a physical *d*-electron count higher than 8.[31] Following the experimentally-calibrated computational approach employed by Lancaster, we found that the LUMOs of **L**CuX

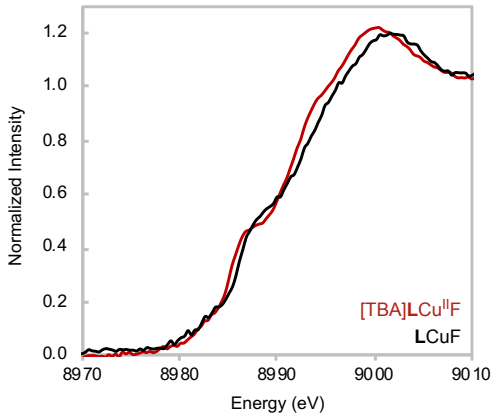


**Figure 4.** Copper K-edge X-ray absorption spectra of [TBA]**L**$Cu^{II}$F (red) and **L**CuF (black) in $CH_2Cl_2$ at 10K.

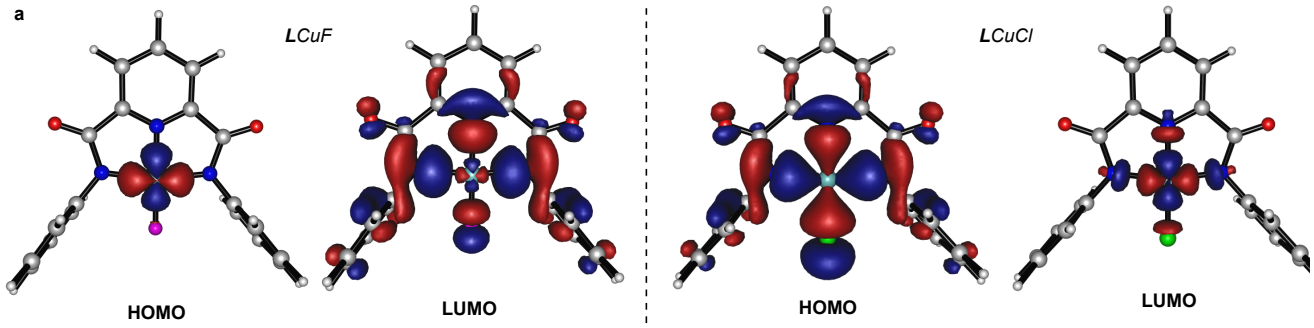


b

| Electronic Structure | LCuF | LCuCl | LCuBr |
|---|---|---|---|
| $Cu^{II}$-X• (%) | 73.9 | 65.4 | 73.3 |
| $Cu^{I}$-$X^{+}$ (%) | 21.5 | 0.6 | 2.2 |
| $Cu^{III}$-$X^{-}$ (%) | 4.6 | 34.0 | 24.5 |

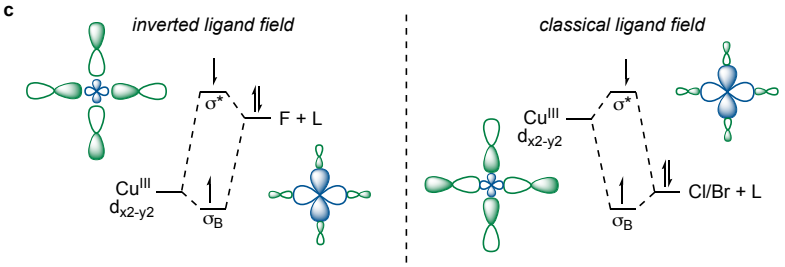


**Figure 5.** (a) Localized HOMO and LUMO from the CASSCF(2 electrons, 2 orbitals) calculation of a truncated model of **L**CuF in which isopropyl groups are substituted with hydrogens. Orbitals are shown at an isovalue of 0.03. (b) Contributions of electronic configurations to the ground state of **L**CuX complexes determined by CASSCF calculations.

complexes are 62.5%, 64.8%, and 66.1% ligand-based for **L**CuF, **L**CuCl, and **L**CuBr, respectively (Figure S51), indicative of significant **L** and halide hole character.

Multireference calculations with the complete active space self-consistent field (CASSCF)[41] method lend further insight into the electronic structure of the $[Cu^{III}\text{-}X]^{2+}$ unit as a function of halide identity. Some of us[42] and others[43] have shown that CASSCF computations can provide valuable insights into the electronic structure of highly covalent metal-ligand interactions. An active space of 2e, 2o (2 electrons, 2 orbitals) comprised of σ bonding and antibonding interactions between the Cu $d_{x2-y2}$ and **L**/halides orbitals (Figure S49) was found to be optimal for this system (see Supplementary Information). State-specific CASSCF calculations reveal that singlet **L**CuX complexes exhibit increasing multireference character and Cu-X covalency (Table S11) from **L**CuF to **L**CuCl to **L**CuBr with increasing σ* population: 0.155 $e^-$ (**L**CuF), 0.172 $e^-$ (**L**CuCl), and 0.189 $e^-$ (**L**CuBr). To assist a valence bond-like interpretation of the CASSCF wave function, the CASSCF(2,2) orbitals were localized with an intrinsic atomic orbitals (IAO) localization method. Subsequent recalculation of the CAS wavefunction permitted delineation of the **L**CuX CAS wavefunction as a combination of various resonance structures: $Cu^{III}$-$X^{-}$, $Cu^{II}$-X•, and $Cu^{I}$-$X^{+}$.[44] In the cases of **L**CuCl and **L**CuBr, the localized HOMO is ligand-centered while the LUMO is copper-centered (Figure 5a). However, the ligand field of **L**CuF is inverted, evidenced by the copper-centered HOMO and ligand-centered LUMO.[30,31] Despite these differences, the leading electronic configuration of all complexes is copper(II) bound to a ligand-centered radical, denoted $Cu^{II}$-X• (Figure 5b). Interestingly, while the second leading configuration of **L**CuCl and **L**CuBr is $Cu^{III}$-$X^{-}$, that of **L**CuF is $Cu^{I}$-$X^{+}$, reflecting the contribution of the inverted ligand field. These interactions can be described with a simplified molecular orbital diagram (Figure 5c). In the case of **L**CuF, the high effective nuclear charge of formally copper(III) lowers the copper orbital energy below the SALC of F and **L**. Taken together, the XAS data and CASSCF calculations support that the oxidation of $[\mathbf{L}Cu^{II}X]^{-}$ to **L**CuX is well distributed over copper and ligands.

**Hydrogen Atom Abstraction and Radical Capture Reactivity of $[Cu^{III}\text{-}X]^{2+}$.** The presence of fluorine radical character in **L**CuF motivated us to explore C($sp^3$)–H fluorination reactivity by the proposed HAA/RC mechanism. Furthermore, previous work by Mcdonald illustrated that bis-carboxamidopyridine nickel chloride complexes is capable of performing HAA.[45] To first understand how electronic structures govern HAA reactivity across the copper(III) halide series, we investigated the reaction of **L**CuX complexes with the hydrogen atom donor, 9,10-dihydroanthracene (DHA). Addition of 100 equivalents of DHA to **L**CuX complexes at −30 °C leads to their consumption with formation of anthracene as revealed by UV-Vis spectroscopy (Figure S12). To confirm that the $\mathbf{L}Cu^{II}$ core remains intact after HAA, the reaction of **L**CuF with DHA was repeated in a scintillation vial. Following workup in acetonitrile, the brown-colored $\mathbf{L}Cu^{II}$(MeCN) complex was isolated in 84% spectroscopic yield (Figure S13). The second-order rate constant ($k$) of HAA was obtained by monitoring the decay of LMCT bands of **L**CuX (820 nm for **L**CuF, 920 nm for **L**CuCl, 980 nm for **L**CuBr, respectively) under pseudo-first-order conditions (see Supplementary Information). The rate of HAA from DHA for **L**CuF is $k$ = 0.668 $M^{-1}$ $s^{-1}$, which is greater than 200 times higher than both **L**CuCl and **L**CuBr (Figure 6). The rapid rate of HAT by **L**CuF is intriguing considering **L**CuF is a weaker oxidant than **L**CuCl and **L**CuBr. Since **L**CuF is expected to be more basic

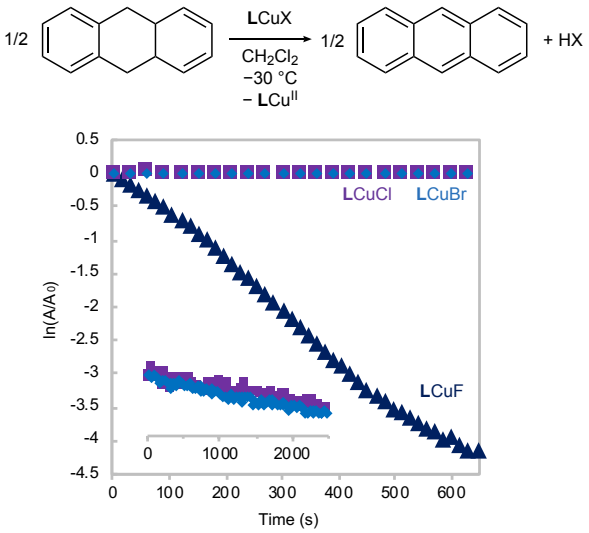


**Figure 6.** Kinetic traces of the reaction between copper(III) halides and 9,10-dihydroanthracene (100 eq, −30 °C).

than **L**CuCl and **L**CuBr, the higher HAA reactivity of **L**CuF can be attributed to the underlying correlation between HAA and basicity of the complex, which was first demonstrated by Tolman's highly basic **L**CuOH complexes.[34]

The difference in HAA reactivity of **L**CuF and **L**CuOH (36x higher) was further probed with an Eyring analysis (ln(*k*/T) vs 1/T). Although **L**CuF exhibits a slightly lower activation enthalpy than **L**CuOH ($\Delta H^{\ddagger}$(**L**CuF) = 3.8(2); $\Delta H^{\ddagger}$(**L**CuOH) = 5.4(2) kcal mol$^{-1}$), there is a greater entropic penalty for **L**CuF ($\Delta S^{\ddagger}$(**L**CuF) = −10(1) cal K$^{-1}$ mol$^{-1}$; $\Delta S^{\ddagger}$(**L**CuOH) = −7.2(5) cal K$^{-1}$ mol$^{-1}$; see Supplementary Information). Despite **L**CuF being ~540 mV more oxidizing than **L**CuOH, the lower basicity of fluoride results in a lower HAA rate, clearly emphasizing the importance of the proton transfer over electron transfer for the overall rate of HAA from DHA by formally **L**Cu$^{III}$ species. In this context, it is informative to compare the HAA rate constants of **L**CuX with **L**CuOH[34] and **L**Cu(O$_2$CR)[46] complexes. Despite the different solvents used for HAA kinetic study, a positive correlation of log(*k*) from HAA by **L**Cu$^{III}$ species with the p$K_a$ of the ligand is observed (Figure S15). However, we recognize that basicity is unlikely to be the only contributing factor, especially as the Cu-X covalency also changes as a function of X.[47,48]

Having established the high rate of HAA by **L**CuF, we were eager to explore the possibility of radical capture as the terminating step in a C(sp$^3$)–H fluorination sequence. A common strategy to explore the capture of alkyl radical (R•) is to examine the reaction of metal complexes with carbon-centered radical precursors e.g. azo compounds and acyl peroxides.[49,50] Heating **L**CuX complexes in the presence of azobisisobutyronitrile (AIBN) at 80 °C in $CD_2Cl_2$ results in the formation of 2-haloisobutyronitriles in 45% (**L**CuF), 60% (**L**CuCl), and 68% (**L**CuBr) yield, respectively (Scheme 2). In contrast, treatment of [TBA]**L**Cu$^{II}$X complexes with AIBN at 80 °C for 2 hours does not furnish halogenated products, consistent with the increased hole character on halides upon oxidation of Cu$^{II}$ to Cu$^{III}$. The lower yield of halogenated product for **L**CuF relative to **L**CuCl and **L**CuBr is likely due to its higher rate of

**Scheme 2. Heating azobisisobutyronitrile (AIBN) in the presence of LCuX complexes furnishes C(sp$^3$)–X bonds**

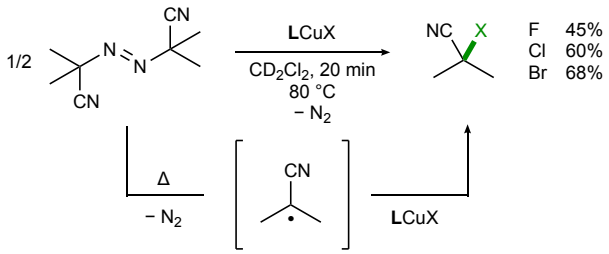


self-decomposition at 80 °C (Figure S16). These results show that discrete [Cu$^{III}$-X]$^{2+}$ complexes mediate carbon radical capture, which has been previously proposed in copper-catalyzed C(sp$^3$)–H halogenation reactions.[28]

To gain insights into the mechanism of radical capture by **L**CuX complexes, we employed trityl radical, generated from the dissociation of Gomberg's dimer.[51,52] Contrary to the two-hundred-fold rate difference for HAA, all **L**CuX complexes react with trityl radical at similar rates at −80 °C. $^1$H NMR analysis of the same reactions at a larger scale confirms the formation of the corresponding $Ph_3C$-F, $Ph_3C$-Cl, and $Ph_3C$-Br products in 86%, 79% and 72% yield, respectively (Figure 7a). Despite the similar efficiency of RC for all three **L**CuX complexes, there are key mechanistic differences. Careful examination of *in situ* UV-Vis profiles reveals that trityl radical capture by **L**CuCl and **L**CuBr proceeds through the trityl cation intermediate ($\lambda_{max}$ = 415 nm), while that by **L**CuF does not (Figure 7b, Figure S17). This result suggests a stepwise electron transfer-halide transfer (ET-XT) mechanism for **L**CuCl and **L**CuBr and a synchronous fluorine atom transfer mechanism for **L**CuF. These observations are consistent with the lower redox potential and higher nucleophilicity of **L**CuF compared to **L**CuCl and **L**CuBr. There is ambiguity in the literature about the suitability of copper(III) versus copper(II)

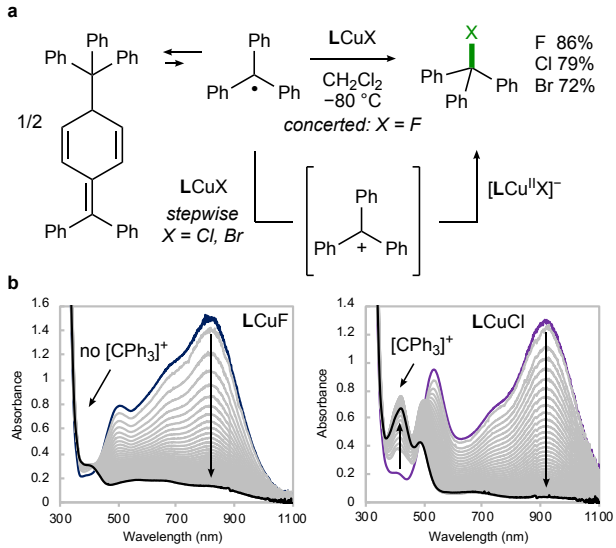


**Figure 7.** (a) Radical capture reactivity study with triphenylmethyl radical at −80 °C reveals the intermediacy of triphenylmethyl cation for **L**CuCl, but not for **L**CuF. (b) UV-Vis traces of the reaction between **L**CuF and **L**CuCl with 1 equivalent of trityl radical (0.1mM, $CH_2Cl_2$, −80 °C).

**Table 1.** Direct C($sp^3$)–H fluorination by **L**CuF[a]

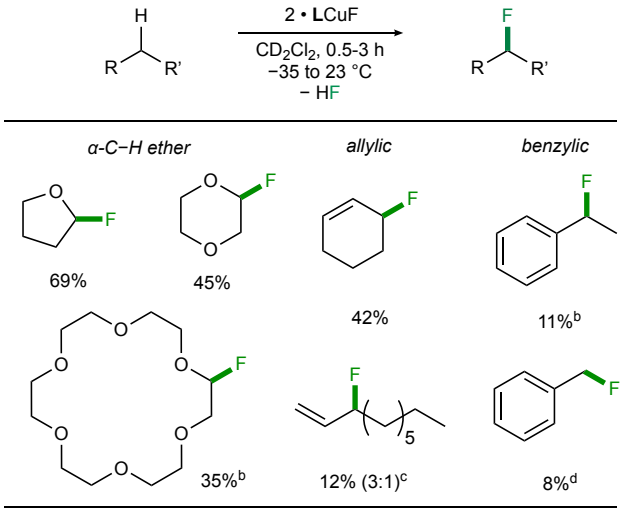


[a]Yields determined by $^{19}F\{^1H\}$ NMR analysis with 100 equivalents of substrate. [b]With 16 equivalents of substrate. [c]Combined yield of branched and linear isomers. [d]After 64 hours.

for alkyl radical capture and whether the precise mechanism is concerted or stepwise.[28,53] Further kinetic studies to quantitate the synchronicity of radical capture by formally copper(III) species are ongoing and will be reported in due course.

**C-H Fluorination Reactivity.** The proficiency of **L**CuF for both hydrogen atom abstraction and radical capture led us to envision the possibility of direct C($sp^3$)–H fluorination by a sequential HAA/RC mechanism. Treatment of **L**CuF with 100 equivalents of tetrahydrofuran at room temperature for 3 hours resulted in the selective formation of 2-fluorotetrahydrofuran in 69% yield based on the requirement of two **L**CuF complexes to furnish one fluorinated product. Fluorination of 1,4-dioxane and 18-crown-6 with **L**CuF proceeds selectively to furnish monofluorinated products formed in 45% and 35% yield, respectively (Table 1). Fluorine atom transfer from a metal fluoride to the α-position of ether, to our knowledge, has yet to be demonstrated. Such direct fluorination by **L**CuF is also amenable to other activated C($sp^3$)–H bonds. Treatment of **L**CuF with allylic and benzylic substrates selectively afforded the corresponding allylic or benzylic fluorinated compounds, albeit in moderate to low yields (8 – 42%, Table 1). The low yield of benzylic substrates suggests that steric hinderance by the four iPr moieties around the $[Cu^{III}\text{-}F]^{2+}$ unit might be detrimental to C($sp^3$)–H fluorination reactivity. This demonstration of C($sp^3$)–H fluorination, despite requiring stoichiometric amount of **L**CuF, suggests that copper fluoride complexes that support the $Cu^{II}/Cu^{III}$ redox couple, in principle, are suitable for fluorination of C($sp^3$)–H bonds with an oxidant and $F^-$ source.

## SUMMARY AND CONCLUSIONS

In summary, we have synthesized a series of formally copper(III) halide complexes, **L**CuX (X = F, Cl, Br), by the use of halide ($X^-$) sources and an oxidant. The electronic structure of these species, as shown by a suite of spectroscopic and computational techniques, features significant halogen radical character, which relates to their ability to perform hydrogen atom abstraction and radical capture. Expanding on these insights, **L**CuF was employed for the direct fluorination of a variety of alkyl substrates with allylic and benzylic C-H bonds as well as α-C–H bonds of ethers. With the establishment of a radical capture mechanism at a copper(III) fluoride center, the use of tunable copper complexes, in principle, can provide further practicality and generality to C($sp^3$)–H fluorination, i.e. regioselectivity and stereoselectivity.

Our demonstration of C($sp^3$)–H fluorination with **L**CuF adds to the growing list of formally copper(III) intermediates in biological[54,55] and abiological[56,57] copper-mediated carbon-heteroatom bond-forming reactions. Conceivably, the generality of this $Cu^{II}/Cu^{III}$ C($sp^3$)–H functionalization paradigm relies on the ability of **L**CuX to abstract H atoms (depending on p$K_a$) and capture R• (depending on redox potential, $E_{1/2}$).[52] Therefore, an interesting mechanistic question arises from the inverse correlation of p$K_a$ and $E_{1/2}$ of **L**CuX – can the **L**CuX complex be efficient at RC and HAA at the same time? As shown by our study, the efficiency of R• capture remains high even with less oxidizing **L**CuX, e.g. **L**CuF. Albeit through two different mechanisms (concerted for **L**CuF, stepwise ET-XT for **L**CuCl and **L**CuBr), the high proficiency of RC at different **L**CuX raises the possibility of realizing other mechanistically related C($sp^3$)–H functionalization with $[Cu^{III}\text{-}X]^{2+}$ species.

## ASSOCIATED CONTENT

The Supporting information is available free of charge on the ACS Publications website at DOI:.

Experimental details, including characterization data, spectra, kinetic data, computational procedures and results.
Crystallographic data for [PPN]**L**$Cu^{II}$F (1985735)
Crystallographic data for [TBA]**L**$Cu^{II}$Cl (19857356)
Crystallographic data for [TBA]**L**$Cu^{II}$Br (1985737)
Crystallographic data for **L**CuF (1985738)
Crystallographic data for **L**CuCl (1985739)
Crystallographic data for **L**CuBr (1985740)

## AUTHOR INFORMATION


### Corresponding Author

*zhang.8941@osu.edu
*sestieber@cpp.edu


## AUTHOR CONTRIBUTION

### Notes

The authors declare no competing financial interest.

## ACKNOWLEDGMENT


This material is based on work supported by the U.S. National Science Foundation under award no. CHE-1904560 (S.Z.) and CHE-1847926 (S.C.E.S.). The authors thank The Ohio State University Department of Chemistry and Biochemistry for additional financial support. High performance computing resources were provided by the Ohio Supercomputer Center. Use of the Stanford Synchrotron Radiation Lightsource, SLAC National Accelerator Laboratory, is supported by the U.S. Department of Energy, Office of Science, Office of Basic Energy Sciences under Contract No. DE-AC02-76SF00515. The authors also thank Dr. Curtis E. Moore

for X-ray crystallography assistance and Madison R. Tuttle for help with EPR simulation.

## REFERENCES


(1) Cheng, Q.; Ritter, T. New Directions in C–H Fluorination. *Trends Chem.* **2019**, *1*, 461–470.

(2) Müller, K.; Faeh, C.; Diederich, F. Fluorine in Pharmaceuticals: Looking beyond Intuition. *Science* **2007**, *317*, 1881–1886.

(3) McMurtrey, K. B.; Racowski, J. M.; Sanford, M. S. Pd-Catalyzed C–H Fluorination with Nucleophilic Fluoride. *Org. Lett.* **2012**, *14*, 4094–4097.

(4) Braun, M.-G.; Doyle, A. G. Palladium-Catalyzed Allylic C–H Fluorination. *J. Am. Chem. Soc.* **2013**, *135*, 12990–12993.

(5) Zhu, R.-Y.; Tanaka, K.; Li, G.-C.; He, J.; Fu, H.-Y.; Li, S.-H.; Yu, J.-Q. Ligand-Enabled Stereoselective β-C($sp^3$)–H Fluorination: Synthesis of Unnatural Enantiopure Anti-β-Fluoro-α-Amino Acids. *J. Am. Chem. Soc.* **2015**, *137*, 7067–7070.

(6) Zhang, Q.; Yin, X.-S.; Chen, K.; Zhang, S.-Q.; Shi, B.-F. Stereoselective Synthesis of Chiral β-Fluoro α-Amino Acids via Pd(II)-Catalyzed Fluorination of Unactivated Methylene C($sp^3$)–H Bonds: Scope and Mechanistic Studies. *J. Am. Chem. Soc.* **2015**, *137*, 8219–8226.

(7) Bloom, S.; Pitts, C. R.; Miller, D. C.; Haselton, N.; Holl, M. G.; Urheim, E.; Lectka, T. A Polycomponent Metal-catalyzed Aliphatic, Allylic, and Benzylic Fluorination. *Angew. Chem. Int. Ed.* **2012**, *51*, 10580–10583.

(8) Bloom, S.; Pitts, C. R.; Woltornist, R.; Griswold, A.; Holl, M. G.; Lectka, T. Iron(II)-Catalyzed Benzylic Fluorination. *Org. Lett.* **2013**, *15*, 1722–1724.

(9) Amaoka, Y.; Nagatomo, M.; Inoue, M. Metal-Free Fluorination of C($sp^3$)–H Bonds Using a Catalytic N-Oxyl Radical. *Org. Lett.* **2013**, *15*, 2160–2163.

(10) Xia, J. B.; Zhu, C.; Chen, C. Visible Light-Promoted Metal-Free C-H Activation: Diarylketone-Catalyzed Selective Benzylic Mono- and Difluorination. *J. Am. Chem. Soc.* **2013**, *135*, 17494–17500.

(11) Xu, P.; Guo, S.; Wang, L.; Tang, P. Silver-Catalyzed Oxidative Activation of Benzylic C-H Bonds for the Synthesis of Difluoromethylated Arenes. *Angew. Chem. Int. Ed.* **2014**, *53*, 5955–5958.

(12) Capilato, J. N.; Pitts, C. R.; Rowshanpour, R.; Dudding, T.; Lectka, T. Site-Selective Photochemical Fluorination of Ketals: Unanticipated Outcomes in Selectivity and Stability. *J. Org. Chem.* **2020**, *85*, 2855–2864.

(13) Rueda-Becerril, M.; Chatalova Sazepin, C.; Leung, J. C. T.; Okbinoglu, T.; Kennepohl, P.; Paquin, J.-F.; Sammis, G. M. Fluorine Transfer to Alkyl Radicals. *J. Am. Chem. Soc.* **2012**, *134*, 4026–4029.

(14) Nodwell, M. B.; Bagai, A.; Halperin, S. D.; Martin, R. E.; Knust, H.; Britton, R. Direct Photocatalytic Fluorination of Benzylic C-H Bonds with N-Fluorobenzenesulfonimide. *Chem. Commun.* **2015**, *51*, 11783–11786.

(15) West, J. G.; Bedell, T. A.; Sorensen, E. J. The Uranyl Cation as a Visible-Light Photocatalyst for C($sp^3$)–H Fluorination. *Angew. Chem. Int. Ed.* **2016**, *55*, 8923–8927.

(16) Groendyke, B. J.; AbuSalim, D. I.; Cook, S. P. Iron-Catalyzed, Fluoroamide-Directed C–H Fluorination. *J. Am. Chem. Soc.* **2016**, *138*, 12771–12774.

(17) Pinter, E. N.; Bingham, J. E.; Abusalim, D. I.; Cook, S. P. N-Directed Fluorination of Unactivated $Csp^3$-H Bonds. *Chem. Sci.* **2020**, *11*, 1102–1106.

(18) Liu, W.; Huang, X.; Cheng, M.-J.; Nielsen, R. J.; Goddard, W. A.; Groves, J. T. Oxidative Aliphatic C-H Fluorination with Fluoride Ion Catalyzed by a Manganese Porphyrin. *Science* **2012**, *337*, 1322–1325.

(19) Liu, W.; Groves, J. T. Manganese-catalyzed Oxidative Benzylic C–H Fluorination by Fluoride Ions. *Angew. Chem. Int. Ed.* **2013**, *52*, 6024–6027.

(20) Huang, X.; Liu, W.; Ren, H.; Neelamegam, R.; Hooker, J. M.; Groves, J. T. Late Stage Benzylic C–H Fluorination with [$^{18}$F]Fluoride for PET Imaging. *J. Am. Chem. Soc.* **2014**, *136*, 6842–6845.

(21) Park, H.; Verma, P.; Hong, K.; Yu, J.-Q. Controlling Pd(IV) Reductive Elimination Pathways Enables Pd(II)-Catalysed Enantioselective C($sp^3$)–H Fluorination. *Nat. Chem.* **2018**, *10*, 755–762.

(22) Liu, J.; Yuan, Q.; Toste, F. D.; Sigman, M. S. Enantioselective Construction of Remote Tertiary Carbon–Fluorine Bonds. *Nat. Chem.* **2019**, *11*, 710–715.

(23) Kainz, Q. M.; Matier, C. D.; Bartoszewicz, A.; Zultanski, S. L.; Peters, J. C.; Fu, G. C. Asymmetric Copper-Catalyzed C-N Cross-Couplings Induced by Visible Light. *Science* **2016**, *351*, 681–684.

(24) Zhang, W.; Wang, F.; McCann, S. D.; Wang, D.; Chen, P.; Stahl, S. S.; Liu, G. Enantioselective Cyanation of Benzylic C–H Bonds via Copper-Catalyzed Radical Relay. *Science* **2016**, *353*, 1014–1018.

(25) Zhang, Z.; Zhang, X.; Nagib, D. A. Chiral Piperidines from Acyclic Amines via Enantioselective, Radical-Mediated δ C–H Cyanation. *Chem* **2019**, *5*, 3127–3134.

(26) Kochi, J. K. The Reduction of Cupric Chloride by Carbonyl Compounds. *J. Am. Chem. Soc.* **1955**, *77*, 5274–5278.

(27) Castro, C. E.; Gaughan, E. J.; Owsley, D. C. Cupric Halide Halogenations. *J. Org. Chem.* **1965**, *30*, 587–592.

(28) Liu, T.; Myers, M. C.; Yu, J. Copper-catalyzed Bromination of C($sp^3$)–H Bonds Distal to Functional Groups. *Angew. Chem. Int. Ed.* **2017**, *56*, 306–309.

(29) Pitts, C. R.; Bloom, S.; Woltornist, R.; Auvenshine, D. J.; Ryzhkov, L. R.; Siegler, M. A.; Lectka, T. Direct, Catalytic Monofluorination of $sp^3$ C–H Bonds: A Radical-Based Mechanism with Ionic Selectivity. *J. Am. Chem. Soc.* **2014**, *136*, 9780–9791.

(30) Hoffmann, R.; Alvarez, S.; Mealli, C.; Falceto, A.; Cahill, T. J.; Zeng, T.; Manca, G. From Widely Accepted Concepts in Coordination Chemistry to Inverted Ligand Fields. *Chem. Rev.* **2016**, *116*, 8173–8192.

(31) DiMucci, I. M.; Lukens, J. T.; Chatterjee, S.; Carsch, K. M.; Titus, C. J.; Lee, S. J.; Nordlund, D.; Betley, T. A.; MacMillan, S. N.; Lancaster, K. M. The Myth of $d^8$ Copper(III). *J. Am. Chem. Soc.* **2019**, *141*, 18508–18520.

(32) Carsch, K. M.; DiMucci, I. M.; Iovan, D. A.; Li, A.; Zheng, S.-L.; Titus, C. J.; Lee, S. J.; Irwin, K. D.; Nordlund, D.; Lancaster, K. M.; Betley, T. A. Synthesis of a Copper-Supported Triplet Nitrene Complex Pertinent to Copper-Catalyzed Amination. *Science* **2019**, *365*, 1138–1143.

(33) Badiei, Y. M.; Dinescu, A.; Dai, X.; Palomino, R. M.; Heinemann, F. W.; Cundari, T. R.; Warren, T. H. Copper–Nitrene Complexes in Catalytic C–H Amination. *Angew. Chem. Int. Ed.* **2008**, *47*, 9961–9964.

(34) Donoghue, P. J.; Tehranchi, J.; Cramer, C. J.; Sarangi, R.; Solomon, E. I.; Tolman, W. B. Rapid C–H Bond Activation by a Monocopper(III)–Hydroxide Complex. *J. Am. Chem. Soc.* **2011**, *133*, 17602–17605.

(35) Yang, L.; Powell, D. R.; Houser, R. P. Structural Variation in Copper(I) Complexes with Pyridylmethylamide Ligands: Structural Analysis with a New Four-Coordinate Geometry Index, $\tau^4$. *Dalton Trans.* **2007**, 955–964.

(36) Casitas, A.; King, A. E.; Parella, T.; Costas, M.; Stahl, S. S.; Ribas, X. Direct Observation of $Cu^{I}/Cu^{III}$ Redox Steps Relevant to Ullmann-Type Coupling Reactions. *Chem. Sci.* **2010**, *1*, 326–330.

(37) Santo, R.; Miyamoto, R.; Tanaka, R.; Nishioka, T.; Sato, K.; Toyota, K.; Obata, M.; Yano, S.; Kinoshita, I.; Ichimura, A.; Takui, T. Diamagnetic–Paramagnetic Conversion of Tris(2-Pyridylthio)Methylcopper(III) through a Structural Change from Trigonal Bipyramidal to Octahedral. *Angew. Chem. Int. Ed.* **2006**, *45*, 7611–7614.

(38) Chang, H.-C.; Lo, F.-C.; Liu, W.-C.; Lin, T.-H.; Liaw, W.-F.; Kuo, T.-S.; Lee, W.-Z. Ambient Stable Trigonal Bipyramidal Copper(III) Complexes Equipped with an Exchangeable Axial Ligand. *Inorg. Chem.* **2015**, *54*, 5527–5533.

(39) DuBois, J. L.; Mukherjee, P.; Stack, T. D. P.; Hedman, B.; Solomon, E. I.; Hodgson, K. O. A Systematic K-Edge X-Ray

Absorption Spectroscopic Study of Cu(III) Sites. *J. Am. Chem. Soc.* **2000**, *122*, 5775–5787.

(40) Tomson, N. C.; Williams, K. D.; Dai, X.; Sproules, S.; DeBeer, S.; Warren, T. H.; Wieghardt, K. Re-Evaluating the Cu K Pre-Edge XAS Transition in Complexes with Covalent Metal–Ligand Interactions. *Chem. Sci.* **2015**, *6*, 2474–2487.

(41) Werner, H. J.; Knowles, P. J. A Second Order Multiconfiguration SCF Procedure with Optimum Convergence. *J. Chem. Phys.* **1985**, *82*, 5053–5063.

(42) Bower, J. K.; Sokolov, A. Y.; Zhang, S. Four-Coordinate Copper Halonitrosyl $\{CuNO\}^{10}$ Complexes. *Angew. Chem. Int. Ed.* **2019**, *58*, 10225–10229.

(43) In-Iam, A.; Wolf, M.; Wilfer, C.; Schaniel, D.; Woike, T.; Klüfers, P. $\{FeNO\}^7$-Type Halogenido Nitrosyl Ferrates: Syntheses, Bonding, and Photoinduced Linkage Isomerism. *Chem. Eur. J.* **2019**, *25*, 1304–1325.

(44) Radoń, M.; Broclawik, E.; Pierloot, K. Electronic Structure of Selected $\{FeNO\}^7$ Complexes in Heme and Non-Heme Architectures: A Density Functional and Multireference Ab Initio Study. *J. Phys. Chem. B* **2010**, *114*, 1518–1528.

(45) Mondal, P.; Pirovano, P.; Das, A.; Farquhar, E. R.; McDonald, A. R. Hydrogen Atom Transfer by a High-Valent Nickel-Chloride Complex. *J. Am. Chem. Soc.* **2018**, *140*, 1834–1841.

(46) Mandal, M.; Elwell, C. E.; Bouchey, C. J.; Zerk, T. J.; Tolman, W. B.; Cramer, C. J. Mechanisms for Hydrogen-Atom Abstraction by Mononuclear Copper(III) Cores: Hydrogen-Atom Transfer or Concerted Proton-Coupled Electron Transfer? *J. Am. Chem. Soc.* **2019**, *141*, 17236–17244.

(47) Pirovano, P.; Farquhar, E. R.; Swart, M.; McDonald, A. R. Tuning the Reactivity of Terminal Nickel(III)-Oxygen Adducts for C-H Bond Activation. *J. Am. Chem. Soc.* **2016**, *138*, 14362–14370.

(48) Elwell, C. E.; Mandal, M.; Bouchey, C. J.; Que, L.; Cramer, C. J.; Tolman, W. B. Carboxylate Structural Effects on the Properties and Proton-Coupled Electron Transfer Reactivity of $[CuO_2CR]^{2+}$ Cores. *Inorg. Chem.* **2019**, *58*, 15872–15879.

(49) Salvador, T. K.; Arnett, C. H.; Kundu, S.; Sapiezynski, N. G.; Bertke, J. A.; Raghibi Boroujeni, M.; Warren, T. H. Copper Catalyzed $sp^3$ C–H Etherification with Acyl Protected Phenols. *J. Am. Chem. Soc.* **2016**, *138*, 16580–16583.

(50) Bour, J. R.; Ferguson, D. M.; McClain, E. J.; Kampf, J. W.; Sanford, M. S. Connecting Organometallic Ni(III) and Ni(IV): Reactions of Carbon-Centered Radicals with High-Valent Organonickel Complexes. *J. Am. Chem. Soc.* **2019**, *141*, 8914–8920.

(51) Jang, E. S.; McMullin, C. L.; Käß, M.; Meyer, K.; Cundari, T. R.; Warren, T. H. Copper(II) Anilides in $sp^3$ C-H Amination. *J. Am. Chem. Soc.* **2014**, *136*, 10930–10940.

(52) Zaragoza, J. P. T.; Yosca, T. H.; Siegler, M. A.; Moënne-Loccoz, P.; Green, M. T.; Goldberg, D. P. Direct Observation of Oxygen Rebound with an Iron-Hydroxide Complex. *J. Am. Chem. Soc.* **2017**, *139*, 13640–13643.

(53) Kochi, J. K. Mechanisms of Organic Oxidation and Reduction by Metal Complexes. *Science* **1967**, *155*, 415–424.

(54) Abad, E.; Rommel, J. B.; Kästner, J. Reaction Mechanism of the Bicopper Enzyme Peptidylglycine α-Hydroxylating Monooxygenase. *J. Biol. Chem.* **2014**, *289*, 13726–13738.

(55) Cao, L.; Caldararu, O.; Rosenzweig, A. C.; Ryde, U. Quantum Refinement Does Not Support Dinuclear Copper Sites in Crystal Structures of Particulate Methane Monooxygenase. *Angew. Chem. Int. Ed.* **2018**, *57*, 162–166.

(56) Hickman, A. J.; Sanford, M. S. High-Valent Organometallic Copper and Palladium in Catalysis. *Nature* **2012**, *484*, 177–185.

(57) Casitas, A.; Ribas, X. The Role of Organometallic Copper(III) Complexes in Homogeneous Catalysis. *Chem. Sci.* **2013**, *4*, 2301–2318.

Formally Copper(III) Halides

Physical & Electronic Structure

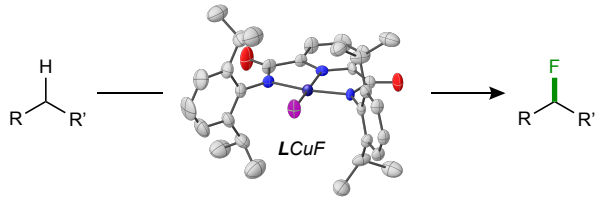


Mechanistic Study

Direct C($sp^3$)-H Fluorination